IEEE Access
Multidisciplinary | Rapid Review | Open Access Journal

Received January 20, 2021, accepted January 31, 2021, date of publication February 3, 2021, date of current version February 10, 2021.

Digital Object Identifier 10.1109/ACCESS.2021.3056797

Subwavelength Racetrack Resonators With Enhanced Critically Coupled Tolerance for On-Chip Sensing

LIJUN HUANG[1], HAI YAN[2], LA XIANG[1], NI ZHOU[1], DAJIANG HE[1], AND XIANWU MI[1]

[1]Key Laboratory of Intelligent Control Technology for Wuling-Mountain Ecological Agriculture in Hunan Province, School of Electrical and Information Engineering, Huaihua University, Huaihua 418008, China

[2]Microelectronic Research Center, Department of Electrical and Computer Engineering, The University of Texas at Austin, Austin, TX 78758, USA

Corresponding authors: Lijun Huang (huanglijun@hhtc.edu.cn), Dajiang He (hdj202@163.com), and Xianwu Mi (xwmi@hotmail.com)

This work was supported in part by the Education Department of Hunan Province under Grant 18B489 and Grant 16A234, in part by the Huaihua University under Grant HHUY2019-10, in part by the China Hunan Provincial Science and Technology Department under Grant 2017NK2074, in part by the NSFC under Grant 11364020, in part by the Key Laboratory of Intelligent Control Technology for Wuling-Mountain Ecological Agriculture in Hunan Province under Grant ZNKZD2019-3, and in part by the Huaihua University Double First-Class initiative Applied Characteristic Discipline of Control Science and Engineering.

ABSTRACT We propose a coupled-tolerant subwavelength photonic racetrack resonator (PRR) on the silicon-on-insulator (SOI) platform, in which a subwavelength grating (SWG) PRR is coupled to a symmetrical SWG bus waveguide. The material equivalent refractive index can be manipulated by the SWG characteristic and thus an additional fabrication degree of freedom can be achieved. The resonant characteristics can be improved significantly by controlling the pillar size and increasing the interaction length between SWG racetrack and bus waveguide (RBW). The simulation results show that the PRR has a high-quality factor and large extinction ratio around 1550nm. Two groups of SWG and strip waveguide (SW) PRRs are fabricated. The fabrication tolerance is tested when fabrication error is changed from 0 to 20 nm and the quality factor is more than 7000 in de-ionized water. The testing results show that the tolerance in SWG-PRR has a 2.0-fold improvement than that in the SW-PRR. Then a fabricated SWG-PRR is employed to monitor different concentration glycerol injected on the chip. An optimal quality factor of 9500 around 1550 nm and bulk sensitivity of 412±0.5 nm/RIU are achieved. Therefore, the structure is a potential candidate for label-free sensing in medical diagnosis and environmental monitoring.

INDEX TERMS Subwavelength structures, gratings, optical sensing and sensors, integrated optics devices.

I. INTRODUCTION

Due to a low power, small size and high sensitivity, optical microring resonators are fundamental building blocks in a broad range of applications in photonics, including optical filters [1], [2], lasers [3], [4], amplifiers [5], multiplexers [6], [7], reflectors [8], modulators [9], [10] and sensors [11]–[18]. Specially, optical microring resonators-based devices have been found promising for the screening of chemical compounds in drug discovery, medical diagnostics, virus detection, food safety, and environment monitoring [19]–[23]. However, the model and resonance spectral features of microring resonators strongly depend on the geometrical parameters and physical effects involved [24]. Thus, it is extremely critical to shape the spectral responses by controlling of the coupling condition between the microrings and waveguides. However, due to the fabrication error and the change of refractive index, there is a challenge when the radius is scaled down to a few micrometers [25]–[27].

Recently, subwavelength grating (SWG) is used to form metamaterial engineered at a microscopic scale to obtain a desired macroscopic phenomenon [28], [29]. On the silicon-on-insulator (SOI) platform, SWG waveguide consists of periodic silicon pillars with a low index material (such as SiO_2 [30], SU-8 polymer [31], air [32] or sensing solution [33]–[37]). The SWG period is smaller than the operating wavelength, so the period structures frustrate diffraction and behave like a homogeneous medium, in which Bragg condition is not satisfied and radiative modes is confined [38]. Also, the light propagation is not only included around the top and side of the waveguide, but also the space between the silicon pillars, so the SWG structure can increase the interaction

The associate editor coordinating the review of this manuscript and approving it for publication was Chao Zuo.

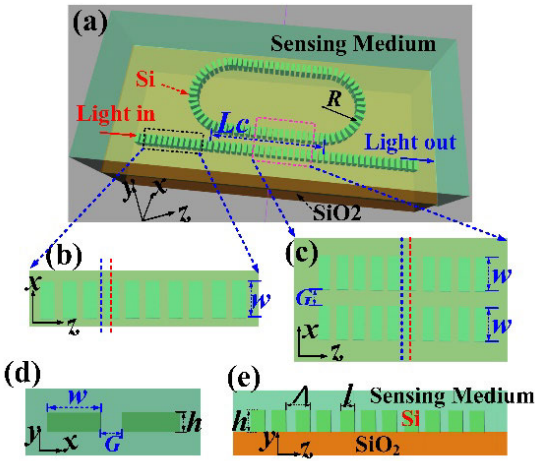

FIGURE 1. (a) The 3D schematic of the proposed SWG-PRR (subwavelength grating photonic racetrack resonator). (b) The magnified image of the SWG bus waveguide in the black dashed box in *xz* plane ($y = 0$). (c) The magnified image between the SWG bus waveguide and racetrack waveguide in the purple dashed box in *xz* plane. (d) The magnified image in the coupled region between the bus and racetrack waveguide in *xy* plane. (e) The image at the middle of SWG bus waveguide in *yz* plane ($x = 0$). L_c: coupling length. *G*: gap. Λ: SWG period. R: radius of racetrack resonator.

region between light and the sensing medium. Therefore, a higher sensitivity is expected. However, for a SWG ring resonator, the coupling length between the SWG bus waveguide and ring resonator is near zero. It is extremely difficult to manipulate the coupling coefficient with a certain gap and silicon pillar size due to the fabrication error [39], [40].

In this article, compared with the strip waveguide (SW) ring resonator and racetrack resonator (RTR) [25], [41], we propose a SWG photonic racetrack resonator (PRR), in which the phase-matching condition is enhanced by manipulating the material equivalent refractive index. We control the coupling condition by manipulating the coupling length and the size of silicon pillars to obtain high performance photonic sensors. Compared with the SWG-PRR and SW-PRR, the tolerance for the fabrication error in SWG-PRR is 2.0 times larger than that in the SW-PRR when a quality factor is more than 7000 and fabrication error is varied from 0 to 20nm. The design will alleviate the stringent requirements for roughness control and lead to cost reduction in manufacturing.

II. DESIGN AND PRINCIPLE

As an integrated optical sensor, the SWG-PRR in SOI platform is primarily designed to detect the change of refractive index (RI) in the solution. The 3D schematic of the proposed SWG-PRR is shown in Fig. 1(a). The origin of the coordinates are the center of SWG bus waveguide (S-BW) in the x, y and z directions. Figure 1(b) is the magnified image of the SWG bus waveguide in the black dashed box in xz plane ($y = 0$). Figure 1(c) represents the partially direction coupling (DC) region between the SWG racetrack and bus waveguide (RBW) in the purple dashed box in xz plane. Figure 1(d) is the magnified image in the coupled region between the RBW in xy plane. Figure 1(e) is the image at the middle of SWG bus waveguide ($x = 0$) in yz plane. The blue partially transparent region on top of the RTR represents the sensing medium with the RI (n_c), and the substrate is SiO_2. The green pillars are silicon (Si) pillars and constitute the SWG bus waveguide. The period (Λ) of SWG is 200 nm, which satisfies the condition $\lambda/\Lambda > 2n_{eff}$ ($\lambda = 1550$ nm). Therefore, the structure operates in the subwavelength regime and behaves like a conventional waveguide [42]. The structural parameters are marked in Fig. 1. The radius (R) is 10μm. l, w and h are the length, width and thickness of silicon (Si) pillars, respectively. L_c and G represent the coupling length and the gap between the RBW and RTR, respectively. The light is entered from the left and output in the right. The coupling efficiency can be precisely controlled by adjusting the size of silicon pillars, the coupling length and gap. Specially, the RTR becomes a ring resonator when the coupling length L_c equals zero.

As shown in Fig.1(b), the basic transmission properties of an all-pass racetrack resonator can be given by [43]

$$\mathrm{T}(\lambda) = \frac{I_{pass}}{I_{input}} = \frac{a^2 - 2atcos(\varphi) + t^2}{1 - 2atcos(\varphi) + (at)^2} \tag{1}$$

a is the single-pass amplitude transmission loss factor, including the propagation loss in the DC region and racetrack region, and can be calculated by the power attenuation coefficient α,

$$a^2 = e^{-i\alpha L} \tag{2}$$

L is the perimeter of the racetrack resonator, and obtained by

$$L = 2\pi R + 2L_c \tag{3}$$

t is the self-coupling coefficient of DC in Eq. (1). Similarly, k can be defined as the cross-coupling coefficient between racetrack and bus waveguide. If there is a negligible optical loss, t and k are assumed to satisfy:

$$t^2 + k^2 = 1 \tag{4}$$

φ is the single-pass phase shift, and is defined as:

$$\varphi = \beta L = \frac{2\pi n_{eff} L}{\lambda} \tag{5}$$

β is the propagation constant of the ring resonator mode, and n_{eff} is the effective refractive index. The resonance of racetrack resonator can be observed when the φ is equal to a multiple of 2π, that is,

$$\lambda_m = \frac{n_{eff} L}{m}, \ m = 1, 2, 3 \ldots \tag{6}$$

Considering the dispersion in the cladding analytes, the change of resonant wavelength ($\Delta\lambda_{\mathrm{res}}$) becomes: [24]

$$\begin{aligned} \Delta\lambda_{res} &= \frac{L}{m}\left[\left(\frac{\delta n_{eff}}{\delta n_c}\right)\Delta c + \left(\frac{\delta n_{eff}}{\delta n_\lambda}\right)\Delta\lambda\right] \\ &= \frac{\lambda_{res}}{n_g}\left(\frac{\delta n_{eff}}{\delta n_c}\right)\Delta c \end{aligned} \tag{7}$$

$$\Delta n_g = \Delta n_{eff} - \lambda\left(\frac{\delta \Delta n_{eff}}{\delta\lambda}\right) \tag{8}$$

n_c represents the RI of cladding analytes. As shown in Eq. (7), the $\Delta\lambda_{\text{res}}$ is related to the change of effective RI with regard to the change of the cladding and the resonant wavelength.

Based on Eq. (1), to achieve the zero transmission at resonance in the high dispersion analytes, the critical coupling condition can be obtained when the coupled power equals the power loss in the racetrack ring. That is:

$$1 - a^2 = k^2 or\ a = t \tag{9}$$

Therefore, a strong resonance can be obtained by achieving a desired cross-coupling coefficient ($k(\lambda_{\text{res}})$), which can be expressed by analyzing the symmetric and anti-symmetric super-modes [44]:

$$k(\lambda) = \sin[\frac{\pi \Delta n(\lambda) L_c}{\lambda}] \tag{10}$$

where the change of RI with wavelength can be given by [45]

$$\Delta n(\lambda) = n_{eff}^{s}(\lambda) - n_{eff}^{as}(\lambda) \tag{11}$$

where $n_{eff}^{s}(\lambda)$ and $n_{eff}^{as}(\lambda)$ are the effective refractive indices of the symmetric and asymmetric modes, respectively. Assumed the optical losses keeps constant in coupling region of racetrack and bus waveguide, and the critically coupled resonant wavelength can be obtained by

$$\lambda_{res} = \frac{\pi L_c \Delta n(\lambda_{res})}{\arcsin[k(\lambda_{res})]} \tag{12}$$

Therefore, the change of λ_{res} is determined by the change among L_c, $\Delta n(\lambda_{\text{res}})$ and $k(\lambda_{\text{res}})$. Based on Eq. (10), the slope of wavelength dependent cross-coupling coefficient can be derived by

$$\frac{dk}{d\lambda} = \frac{\pi L_c}{\lambda^2}(\frac{\lambda d\Delta n(\lambda)}{d\lambda} - \Delta n(\lambda))\cos[\frac{\pi \Delta n(\lambda) L_c}{\lambda}] \tag{13}$$

Considering the critically coupled resonant wavelength, combined with Eq. (8), the Eq. (13) can be derived by

$$\frac{dk}{d\lambda}|_{\lambda=\lambda_{res}} = -\frac{\pi L_c}{\lambda_{res}^2}\Delta n_g\sqrt{1-\kappa_{res}^2} \tag{14}$$

Combined with the Eqs. (12)-(14), the change of the cross-coupling coefficient and resonant wavelength is mostly dominated by the change of coupling length L_c. Based on Eq. (10), the cross-coupling coefficient ($k(\lambda_{\text{res}})$) can be achieved by increasing the coupling length L_c to satisfy the formula:

$$k(\lambda_{res}) = \sin[k\pi + \frac{\pi \Delta n(\lambda) L_c^k}{\lambda}] \tag{15}$$

Equation (15) can be re-arranged by

$$L_c^k = arc\sin[k(\lambda_{res})]\frac{\lambda_{res}}{\pi \Delta n(\lambda_{res})} + \frac{\lambda_{res}}{\Delta n(\lambda_{res})}$$
$$k = 0, 1, 2, 3 \ldots \tag{16}$$

Therefore, combined with the simulation calculations, under certain pillar size and gap between the racetrack and bus waveguide, we can adjust the coupling length to precisely control the cross-coupling coefficient so that the critically coupled resonance is achieved in the RTR [46].

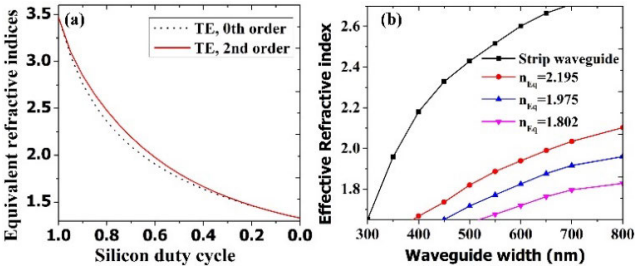

FIGURE 2. (a) The equivalent refractive indices (n_{Eq}) of SWG for different duty cycle; (b) The effective indices of different waveguide width when the n_{Eq} = strip waveguide (3.476), 2.195, 1.975, 1.802, respectively.

The subwavelength grating period in the z axis is smaller than the wavelength of the propagation light, which allows to employ effective medium theory (EMT) at the zeroth-order to approximate the structure [47]. The zeroth-order approximation is only accurate when the period-to-wavelength ratio ($\Lambda \bullet n_{\text{eff}}/\lambda$) is much smaller than 1. Whereas more accurate approximations employing the second-order EMT may be used when the subwavelength period is of the same order as the wavelength in the medium [48]. The formulas of the zero- and second- order approximations of TE modes, and the zero- order approximation of TM mode are expressed by [47]

$$\frac{1}{n_{Eq}^{TE0}} = [\frac{f_{si}}{n_{si}^2} + \frac{1-f_{si}}{n_{clad}^2}]^{\frac{1}{2}} \tag{17}$$

$$n_{Eq}^{TM0} = [f_{si}n_{si}^2 + (1-f_{si})n_{clad}^2]^{\frac{1}{2}} \tag{18}$$

$$n_{Eq}^{TE2} = n_{Eq}^{TE0}\Big[1 + \frac{\pi^2}{3}\frac{\Lambda^2}{\lambda^2}f_{si}^2(1-f_{si})^2\left(n_{si}^2 - n_{clad}^2\right)^2 \times (n_{Eq}^{TM0})^2(\frac{(n_{Eq}^{TE0})^2}{n_{si}^2 n_{clad}^2})^2\Big]^{\frac{1}{2}} \tag{19}$$

The equivalent refractive indices are dependent on silicon duty cycle. The Si duty cycle (η) is defined as the l dividing by Λ. The zero- and second- order approximations of TE modes are shown in Fig. 2(a). As shown in Fig. 2(a), the second-order approximation of TE mode gives more accurate results for the subwavelength grating waveguide when the η equals 0.7 [47], [49]. Figure 2(b) is the effective refractive indices for different equivalent refractive indices with different SWG width. As shown in Fig. 2(b), the effective RI's dependency on waveguide width are significantly different between SWG and the conventional strip waveguide. The slope of curve for SWG is much smaller than the curve for the strip waveguide. Consequently, the phase-matching condition for the strip waveguide will be more sensitive to fabrication variations of the waveguide's width, and will be difficult to precisely control coupling coefficient [50]. Thus, a low rate of change for the effective RI can be achieved when SWG waveguide width is changed. As a result, it is easier to satisfy the coupling condition between racetrack and bus waveguide.

III. DEVICE SIMULATION AND ANALYSIS

To analyze the electric field in the SWG waveguide around 1550 nm, TE mode profiles are simulated in

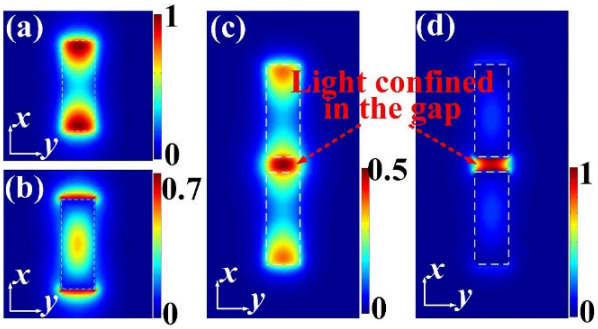

FIGURE 3. Electric fields intensity distribution of TE mode in *xy* plane at blue (a) and red (b) dashed line position in Fig. 1(b). Electric fields intensity distribution of TE mode in *xy* plane in blue (c) and red (d) dashed line position in Fig. 1(c).

RSoft BandSOLVE. The electric field in the SWG bus waveguide (blue and red dash line in Fig. 1(b)) in *xy* plane are shown in Figs. 3(a) and (b), respectively. TE mode profiles at blue and red dash line between SWG racetrack and bus waveguide in *xy* plane in Fig. 1(c) are shown in Figs. 3(c) and 3(d). The dimensions of the silicon pillar in this simulation are $l = 140$ nm, $w = 600$nm, and $h = 220$nm. The Si duty cycle (η) is 0.7. As seen in Fig. 3, the electric field extends into the low refractive index materials in *xy* plane. Specially, the light is squeezed within the slot between the SWG racetrack and bus waveguide. Therefore, due to the fabrication roughness, the distribution of the light in the slot is intensively affected by the change of Si pillars.

We analyze the quality factor (Q) and extinction ratio of the transmission spectra with the change of the dimension of Si pillars based on our previous work [35]. For the silicon pillars in the subwavelength grating racetrack resonator, the grating period is the same as the bus waveguide. The coupling strength and loss are severely affected by the width and length of pillars, the coupling length and gap between SWG-RBW, and radiation loss, *etc*. The simulations are performed with a non-uniform grid to achieve a good accuracy with a reasonable computational workload. The RBW is discretized with $\Delta x/\Delta y/\Delta z = 5$ nm. The grid spacing is gradually increased up to 50 nm for the sensing medium region. Through a parameter scanning in simulation calculations, the L_c and G between the RBW are 8μm and 100 nm to achieve a high quality factor and extinction ratio when $l = 140$ nm, $w = 600$nm, and $h = 220$nm.

The normalized transmissions for different deviation (0 and 20 nm) of pillar width ($n_{Eq} = 2.195$) are shown in Fig. 4(a). The quality (Q) factors as a function of the pillars width variation (σ_S) are shown in Fig. 4(b). As seen, the simulation results show that the Q factor and extinction ratio is large when the pillars width isn't deviated. Whereas that is low when the deviation is increased when the n_{Eq} of the SWG waveguide is the same in Fig. 4(a). As mentioned earlier, the accuracy of critically coupling condition is dis-satisfied with the change of pillars size [27]. Specially, the variance of Q factor is remarkably different for different n_{Eq} waveguide. To maintain a low-quality factor with resonators better than

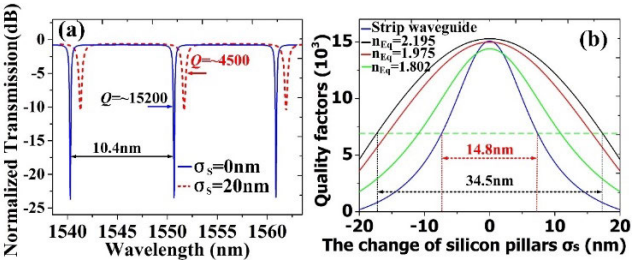

FIGURE 4. (a) The normalized transmission for the deviation (0 and 20 nm) of pillars width when the n_{Eq} of the SWG waveguide is 2.195. The red dashed curve is shifted by 1nm deliberately to show clearly. (b) The Q factors for different n_{Eq} waveguide with the variance of pillars width.

7000 at the central wavelength of 1550nm, it is required to maintain the σ_S is less than 14.8nm, 34.5nm, 30.6nm, 21.2nm, for the strip waveguide and $n_{Eq} = 2.195$, 1.975, 1.802, respectively. The maximum tolerance of the variance for pillars width is achieved at $n_{Eq} = 2.195$ ($\eta = 0.7$), where the maximum Q factor is achieved. Compared with the strip waveguide, the proposed design has a 2.3-fold improvement in the tolerance of pillars size. Furthermore, the variance of extinction ratio is similar to the variance of Q factor for different waveguide [51]. Therefore, according to the Eq. (10) and Fig. 4, the fabrication tolerance of SWG waveguide width can be remarkably improved by engineering the material refractive index of the SWG waveguide [35].

IV. DEVICES FABRICATION AND RESULTS

The proposed SWG-PRR are demonstrated on a SOI wafer with 220 nm thick top silicon layer and 3μm buried oxide (BOX) layer. The device is exposed by the e-beam lithography (EBL), and an inductively coupled plasma reactive ion etching (RIE) process with HBr and Cl_2 is employed to transfer the pattern to silicon layer, in which an acceptable roughness over the silicon slits roughness and nearly vertical side-walls (angle $> 88°$) is accomplished [52], [53]. Some deviations in the fabrication of resonators are expected due to the unavoidable errors, including the variation of waveguide width and gap, slanted waveguide side-walls, etc. We fabricate the devices to obtain the optimal characteristic by scanning the parameter considering the proximity effects.

Based on the simulation results, we fabricated two groups of SWG-PRRs and SW-PRRs by scanning the parameters, respectively. Figures 5(a) and 5(d) show the scanning electron microscopy (SEM) images of a fabricated SWG-PRR and a SW-PRR. Figures 5(b) and 5(c) are the magnified SEM images of the part coupling region of the RBW and the right taper from the strip waveguide to the SWG waveguide, respectively. Figure 5(e) is the magnified SEM image of the part coupling region between the strip RBW. Figure 5(f) is the magnified SEM image of the strip waveguide. As shown in Fig. 5, the coupling length between racetrack and bus waveguide is 8μm, and the radius of the RTR is 10μm. To enhance the coupling efficiency and reduce the mode coupling loss between the strip and SWG waveguide, we design a tapered waveguide of 40 μm to change gradually the SW to SWG waveguide, and a tapered width of the SW (about 6mm

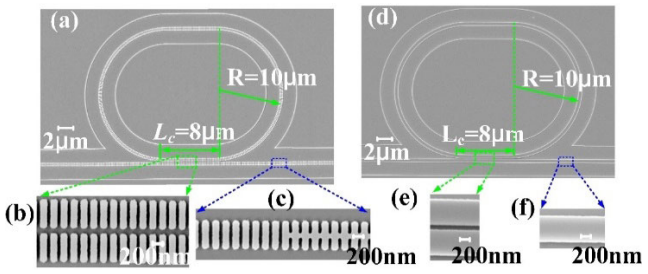

FIGURE 5. (a) The SEM image of a fabricated SWG-PRR. (b) The magnified SEM images between the RBW and (c) the right taper from the SW to the SWG waveguide. (d) The SEM image of a fabricated SW-PRR (strip waveguide photonic racetrack resonator). (e) The magnified SEM image between the strip RBW. (f) The magnified SEM image of the SW.

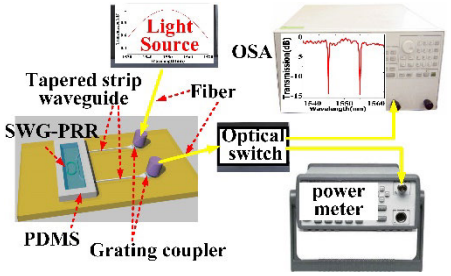

FIGURE 6. The testing schematic of the proposed PRR. PDMS: Polydimethylsiloxane.

of length) from 20 μm at the position of grating coupler to 600nm at the begin of tapered waveguide is designed. Similarly, compare with the PRR, the coupling length between strip RBW is also 8μm, and the radius is 10μm. To satisfy the mode match, the width of the SW is tapered from 20 μm at the position of grating coupler to 600nm at the straight waveguide before the coupling region.

The testing schematic of the proposed PRR is shown in Fig. 6, in which the devices include a 1550 nm super luminescent LED (SLED) source, an optical spectrum analyzer (OSA), the fabricated PRR, a Polydimethylsiloxane (PDMS) microfluidic channel, an optical switch and a power meter. Besides, an automation alignment stage on a temperature controller is also included in the testing process. The fiber and grating coupler are aligned by the automation alignment stage. Light from the SLED is inputted from one terminal of the fiber array, then is coupled to the TE grating coupler on the chip. After the light goes through the resonator, the output light is collected by another terminal of fiber array, and the whole system is connected to an OSA to capture the optical spectra. A PDMS microfluidic channel is integrated on the stage in which the solution is pumped and flowed onto the sensing chip at a controlled flow rate. The temperature Controller thermally controls the temperature of the sensing stage to avoid temperature-induced resonance shift in the sensing process.

The fabricated SWG-PRRs and SW-PRRs are first measured in de-ionized (DI) water. The quality factors are firstly analyzed for the two groups of the fabricated PRRs, and the tested results are shown in Fig. 7. The insets are the SEM images for different coupling gap between the subwavelength

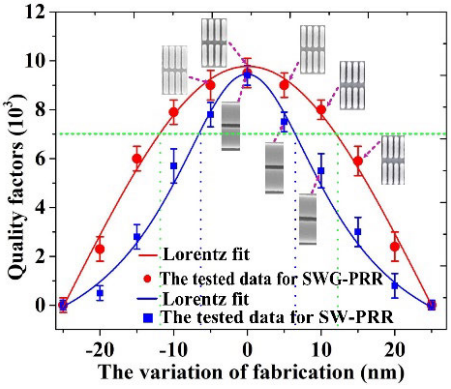

FIGURE 7. The tested quality factors for the SWG-PRRs and SW-PRRs with different simulated fabrication variation.

racetrack and bus waveguide, the coupling gap between the strip racetrack and bus waveguide, respectively. As shown in Fig. 7, the quality factors estimated from the full width at half maximum (FWHM) of the resonance in aqueous solution are changed with the change of simulated fabricated variation. The quality factors are decreased when the gaps are deviated from the optimal distance for the two groups of PRRs. The tested errors are relatively large for different devices with the same gap due to the influence of the fabrication and error estimation in aqueous solution, whereas the influence of the deviation for the SW-PRRs becomes worse compared with the SWG-PRRs. The maximum quality factor for the fabricated PRR is about 9.5×10^3, which is lower than the simulation result. However, the tolerance for the SWG-PRR is about 24.7 nm when the quality factor is more than 7×10^3, whereas it is about 12.3 nm for the SW-PRR. The proposed design has about 2.0-fold improvement in the tolerance. The tolerance in fabrication is slightly different with the result in simulation. The fabrication induced roughness and the error estimation of the resonance are the possible reason for the discrepancy between the simulation and the fabrication. As shown in Fig. 7, the maximum quality factor of $\sim 9.45 \times 10^3$ for the SW-PRR (the roughness of fabrication is 0 nm) tested in aqueous solution is less than that of SWG-PRR, which is also less than the maximum value reported for strip waveguide microring resonators [54]. To compare the variation trend with the fabrication error, the coupling length of the fabricated SWG-PRR and SW-PRR is the same and the critical coupling condition for SW-PRR may be not satisfied. However, the variation trend of quality factor with the deviation of fabrication is the same.

The transmission spectrum of a fabricated SWG-PRR is shown in Fig. 8. As seen in Fig. 8, the optimal quality factor and extinction ratio of the fabricated SWG-PRR are achieved near 1550 nm when $L_c = 8\mu$m, $G = 100$nm, $l = 140$ nm, $w = 600$nm, and $h = 220$nm, respectively. A quality factor of ~9500 at 1545.0nm is obtained by estimating the full-width at half-maximum (FWHM) of the resonance, and the extinction ratio is about 14.8dB. The free spectral range (SPR) is about 10.0nm.

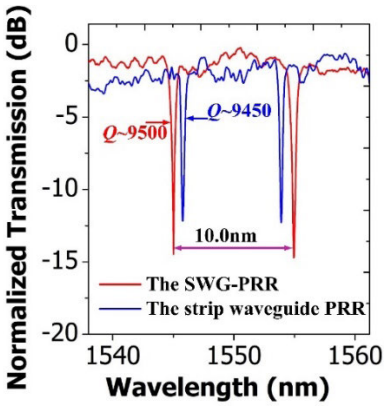

FIGURE 8. The transmission spectra of a fabricated SWG-PRR and a SW-PRR measured in DI water. The transmission spectrum of the SW-PRR is shifted by 1nm deliberately to show clearly.

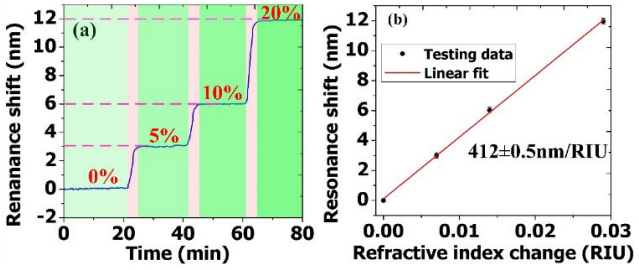

FIGURE 9. (a) The results of the resonance shift for a fabricated SWG-PRR with the monitored time continuously when different concentration glycerol is injected on the chip. (b) The linear fitting plot of the resonance shifts.

For effective assessment of the ability in biochemical sensing, the different concentration glycerol is consecutively injected onto the surface of the fabricated chips with microfluidic channels. The sensitivity of a SWG-PRR is acquired by monitoring the resonance shift. The chip stage is kept at 25°C with a temperature controller. The results monitored by injecting a gradually increased concentration glycerol are shown in Fig. 9(a). As seen, the trend means that the resonance is pushed gradually to a higher-wavelength. The pink regions are the period when new concentration of glycerol solution is inputted gradually, then the solution concentration is increased. The resonance is changed consecutively with a red-shift when a higher-concentration glycerol is employed, and the concentration covering on the chip is increased. Then the resonance is kept at a constant when the concentration covered on the chip is steady. The refractive indices for 0%, 5%, 10%, and 20% glycerol in the solutions are 1.333, 1.340, 1.347 and 1.362, respectively, [55]. Figure 9(b) is the linear fitting of the shift with respect to the change of refractive index of glycerol. The bulk sensitivity (S_b) of the fabricated SWG-PRR is about 412±0.5nm/RIU (refractive index unit). The intrinsic detection limit (*i*DL): $iDL = \Delta n_{\min} = \lambda_{res}/Q \bullet S_b = 3.94 \times 10^{-4}$RIU. The *i*DL is the minimum index change ($\Delta n_{\min}$) required to shift the resonance wavelength by one linewidth ($\Delta\lambda_{3dB}$). Compared with the photonic crystal sensors [56], [57], the proposed SWG-PRR possesses a superiority on-chip sensing due to a large light-matter interaction and higher-sensitivity. Furthermore, the sensitivity of the proposed SWG-PRR can be further enhanced by increasing the mode volume overlap to decrease the pillar duty cycle, the width and the thickness of SWG pillars. However, the challenge of fabrication will be also increased with the decrease of pillar size. The optical loss, especially absorption loss and scattering loss in aqueous solution, will increase inevitably, which can be suppressed by moving to a shorter wavelength of 1310 nm, and the sensor devices would suffer about an order of magnitude less of the absorption loss [24].

V. CONCLUSION

A fabrication-tolerant subwavelength grating photonic racetrack resonator on the SOI platform has been designed and experimentally demonstrated. The SWG period structure was employed to obtain an additional fabrication degree of freedom by manipulating the SWG's equivalent refractive index. The optimal quality factor and extinction ratio of the fabricated SWG-PRR has been achieved near 1550 nm when $L_c = 8\mu$m, $G = 100$nm, $l = 140$ nm, $w = 600$nm, and $h = 220$nm, respectively. The testing results showed that the fabrication tolerance for the SWG-PRR has a 2.0-fold improvement than that in the strip waveguide PRR. A quality factor of 9500 around 1550 nm and sensitivity of 412±0.5nm/RIU in sensing medium are achieved. Therefore, the proposed recipe provides a potential solution for fabrication-tolerance PRRs based on the subwavelength period structure, and alleviate the stringent requirements of roughness control and reduce the costs in manufacturing for on-chip biochemical sensing.

REFERENCES

[1] X. Zhai, S. Wen, D. Xiang, L.-L. Wang, W. Rexidaiguli, L. Wang, and D. Fan, "A subwavelength plasmonic waveguide filter with a ring resonator," *J. Nanomater.*, vol. 2013, Mar. 2013, Art. no. 484207.

[2] J. Wang, I. Glesk, and L. R. Chen, "Subwavelength grating filtering devices," *Opt. Exp.*, vol. 22, no. 13, pp. 15335–15345, Jun. 2014.

[3] H. Chandrahalim, Q. Chen, A. A. Said, M. Dugan, and X. Fan, "Monolithic optofluidic ring resonator lasers created by femtosecond laser nanofabrication," *Lab Chip*, vol. 15, no. 10, pp. 2335–2340, 2015.

[4] T. Chu, N. Fujioka, and M. Ishizaka, "Compact, lower-power-consumption wavelength tunable laser fabricated with silicon photonic-wire waveguide micro-ring resonators," *Opt. Exp.*, vol. 17, pp. 14063–14068, Aug. 2009.

[5] V. M. Menon, W. Tong, and S. R. Forrest, "Control of quality factor and critical coupling in microring resonators through integration of a semiconductor optical amplifier," *IEEE Photon. Technol. Lett.*, vol. 16, no. 5, pp. 1343–1345, May 2004.

[6] A. Vorckel, M. Monster, W. Henschel, P. H. Bolivar, and H. Kurz, "Asymmetrically coupled silicon-on-insulator microring resonators for compact add-drop multiplexers," *IEEE Photon. Technol. Lett.*, vol. 15, no. 7, pp. 921–923, Jul. 2003.

[7] Y. Zhang, X. Qiu, C. Zeng, D. Li, G. Gao, Y. Wang, J. Yu, and J. Xia, "Slow-light dispersion in one-dimensional photonic crystal racetrack ring resonator," *IEEE Photon. Technol. Lett.*, vol. 27, no. 10, pp. 1120–1123, May 15, 2015.

[8] Y. Chung, D.-G. Kim, and N. Dagli, "Reflection properties of coupled-ring reflectors," *J. Lightw. Technol.*, vol. 24, no. 4, pp. 1865–1874, Apr. 2006.

[9] G. Fan, Y. Li, C. Hu, L. Lei, and Y. Guo, "A process to control light in a micro resonator through a coupling modulation by surface acoustic waves," *Sci. Rep.*, vol. 6, no. 1, Nov. 2016, Art. no. 30681.

[10] J. M. Rothenberg, C. P. Chen, J. J. Ackert, J. I. Dadap, A. P. Knights, K. Bergman, R. M. Osgood, and R. R. Grote, "Experimental demonstration of coherent perfect absorption in a silicon photonic racetrack resonator," *Opt. Lett.*, vol. 41, no. 11, pp. 2537–2540, Jun. 2016.

[11] F. Vollmer and L. Yang, "Review label-free detection with high-Q microcavities: A review of biosensing mechanisms for integrated devices," *Nanophotonics*, vol. 1, nos. 3–4, pp. 267–291, Dec. 2012.
[12] P. R. Prasad, S. K. Selvaraja, and M. M. Varma, "High precision measurement of intensity peak shifts in tunable cascaded microring intensity sensors," *Opt. Lett.*, vol. 41, no. 14, p. 3153, Jul. 2016.
[13] S. RoyChoudhury, V. Rawat, A. H. Jalal, S. N. Kale, and S. Bhansali, "Recent advances in metamaterial split-ring-resonator circuits as biosensors and therapeutic agents," *Biosens. Bioelectron.*, vol. 86, pp. 595–608, Dec. 2016.
[14] C.-T. Wang, C.-Y. Wang, J.-H. Yu, I.-T. Kuo, C.-W. Tseng, H.-C. Jau, Y.-J. Chen, and T.-H. Lin, "Highly sensitive optical temperature sensor based on a SiN micro-ring resonator with liquid crystal cladding," *Opt. Exp.*, vol. 24, no. 2, pp. 1002–1007, Jan. 2016.
[15] G. Gao, Y. Zhang, H. Zhang, Y. Wang, Q. Huang, and J. Xia, "Air-mode photonic crystal ring resonator on silicon-on-insulator," *Sci. Rep.*, vol. 6, no. 1, Apr. 2016, Art. no. 19999.
[16] Y. Zou, S. Chakravarty, C.-J. Chung, X. Xu, and R. T. Chen, "Mid-infrared silicon photonic waveguides and devices," *Photon. Res.*, vol. 6, pp. 254–276, Apr. 2018.
[17] G. A. Rodriguez, S. Hu, and S. M. Weiss, "Porous silicon ring resonator for compact, high sensitivity biosensing applications," *Opt. Exp.*, vol. 23, no. 6, pp. 7111–7119, Mar. 2015.
[18] K. D. Vos1, I. Bartolozzi, E. Schacht, P. Bienstman, and R. Baets, "Silicon-on-insulator microring resonator for sensitive and label-free biosensing," *Opt Exp.*, vol. 15, pp. 7610–7615, Jun. 2007.
[19] C.-Y. Chao and L. J. Guo, "Biochemical sensors based on polymer microrings with sharp asymmetrical resonance," *Appl. Phys. Lett.*, vol. 83, no. 8, pp. 1527–1529, Aug. 2003.
[20] J. T. Kindt, M. S. Luchansky, A. J. Qavi, S.-H. Lee, and R. C. Bailey, "Subpicogram per milliliter detection of interleukins using silicon photonic microring resonators and an enzymatic signal enhancement strategy," *Anal. Chem.*, vol. 85, no. 22, pp. 10653–10657, Nov. 2013.
[21] D. Ullien, P. J. Harmsma, S. M. C. Abdulla, B. M. de Boer, D. Bosma, E. J. R. Sudhölter, L. C. P. M. de Smet, and W. F. Jager, "Protein detection on biotin-derivatized polyallylamine by optical microring resonators," *Opt. Exp.*, vol. 22, no. 13, pp. 16585–16594, Jun. 2014.
[22] F. Ghasemi, E. S. Hosseini, X. Song, D. S. Gottfried, M. Chamanzar, M. Raeiszadeh, R. D. Cummings, A. A. Eftekhar, and A. Adibi, "Multiplexed detection of lectins using integrated glycan-coated microring resonators," *Biosens. Bioelectron.*, vol. 80, pp. 682–690, Jun. 2016.
[23] A. Ksendzov and Y. Lin, "Integrated optics ring-resonator sensors for protein detection," *Opt. Lett.*, vol. 30, pp. 3344–3346, Dec. 2005.
[24] H. Mohseni, M. H. Agahi, M. Razeghi, S. Schmidt, J. Flueckiger, W. Wu, S. M. Grist, S. Talebi Fard, V. Donzella, P. Khumwan, E. R. Thompson, Q. Wang, P. Kulik, X. Wang, A. Sherwali, J. Kirk, K. C. Cheung, L. Chrostowski, and D. Ratner, "Improving the performance of silicon photonic rings, disks, and Bragg gratings for use in label-free biosensing," *Proc. SPIE*, vol. 9166, Aug. 2014, Art. no. 91660M.
[25] W. Bogaerts, P. De Heyn, T. Van Vaerenbergh, K. De Vos, S. K. Selvaraja, T. Claes, P. Dumon, P. Bienstman, D. Van Thourhout, and R. Baets, "Silicon microring resonators," *Laser Photon. Rev.*, vol. 6, pp. 47–73, Jan. 2012.
[26] D.-P. Cai, J.-H. Lu, C.-C. Chen, C.-C. Lee, C.-E. Lin, and T.-J. Yen, "High Q-factor microring resonator wrapped by the curved waveguide," *Sci. Rep.*, vol. 5, no. 1, Sep. 2015, Art. no. 10078.
[27] A. Yariv, "Universal relations for coupling of optical power between microresonators and dielectric waveguides," *Electron. Lett.*, vol. 36, no. 4, p. 321, 2000.
[28] P. Cheben, R. Halir, J. H. Schmid, H. A. Atwater, and D. R. Smith, "Subwavelength integrated photonics," *Nature*, vol. 560, no. 7720, pp. 565–572, Aug. 2018.
[29] R. Halir, A. Ortega-Monux, D. Benedikovic, G. Z. Mashanovich, J. G. Wanguemert-Perez, J. H. Schmid, I. Molina-Fernandez, and P. Cheben, "Subwavelength-grating metamaterial structures for silicon photonic devices," *Proc. IEEE*, vol. 106, no. 12, pp. 2144–2157, Dec. 2018.
[30] P. J. Bock, P. Cheben, J. H. Schmid, J. Lapointe, A. Delâge, S. Janz, G. C. Aers, D.-X. Xu, A. Densmore, and T. J. Hall, "Subwavelength grating periodic structures in silicon-on-insulator: A new type of microphotonic waveguide," *Opt. Exp.*, vol. 18, pp. 20251–20262, Sep. 2010.
[31] P. Cheben, P. J. Bock, J. H. Schmid, J. Lapointe, S. Janz, D. Xu, A. Densmore, A. Delâge, B. Lamontagne, and T. J. Hall, "Refractive index engineering with subwavelength gratings for efficient microphotonic couplers and planar waveguide multiplexers," *Opt. Lett.*, vol. 35, pp. 2526–2528, Aug. 2010.
[32] V. Donzella, A. Sherwali, J. Flueckiger, S. Talebi Fard, S. M. Grist, and L. Chrostowski, "Sub-wavelength grating components for integrated optics applications on SOI chips," *Opt. Exp.*, vol. 22, no. 17, pp. 21037–21050, Aug. 2014.
[33] J. Gonzalo Wangemert-Pérez, P. Cheben, A. Ortega-Moñux, C. Alonso-Ramos, D. Pérez-Galacho, R. Halir, I. Molina-Fernández, D.-X. Xu, and J. H. Schmid, "Evanescent field waveguide sensing with subwavelength grating structures in silicon-on-insulator," *Opt. Lett.*, vol. 39, no. 15, p. 4442, Aug. 2014.
[34] J. Flueckiger, S. Schmidt, V. Donzella, A. Sherwali, D. M. Ratner, L. Chrostowski, and K. C. Cheung, "Sub-wavelength grating for enhanced ring resonator biosensor," *Opt. Exp.*, vol. 24, no. 14, pp. 15672–15686, Jul. 2016.
[35] H. Yan, L. Huang, X. Xu, S. Chakravarty, N. Tang, H. Tian, and R. T. Chen, "Unique surface sensing property and enhanced sensitivity in microring resonator biosensors based on subwavelength grating waveguides," *Opt Exp.*, vol. 24, pp. 29724–29733, Dec. 2016.
[36] L. Huang, H. Yan, X. Xu, N. Tang, S. Chakravarty, H. Tian, and R. T. Chen, "Improving the detection limit for on-chip photonic sensors based on subwavelength grating racetrack resonators," *Opt Exp.*, vol. 25, pp. 10527–10535, May 2017.
[37] E. Luan, H. Yun, L. Laplatine, Y. Dattner, D. M. Ratner, K. C. Cheung, and L. Chrostowski, "Enhanced sensitivity of subwavelength multibox waveguide microring resonator label-free biosensors," *IEEE J. Sel. Topics Quantum Electron.*, vol. 25, no. 3, pp. 1–11, May 2019.
[38] P. Yeh, A. Yariv, and C. S. Hong, "Electromagnetic propagation in periodic stratified media. I. General theory," *J. Opt. Soc. Amer. A, Opt. Image Sci.*, vol. 7, pp. 423–438, Apr. 1977.
[39] Z. Wang, X. Xu, D. Fan, Y. Wang, H. Subbaraman, and R. T. Chen, "Geometrical tuning art for entirely subwavelength grating waveguide based integrated photonics circuits," *Sci. Rep.*, vol. 6, no. 1, Jul. 2016, Art. no. 24106.
[40] D.-P. Cai, C.-C. Chen, C.-C. Lee, and T.-D. Wang, "Study of coupling length of concentrically curved waveguides," *IEEE Photon. J.*, vol. 4, no. 1, pp. 80–85, Feb. 2012.
[41] W. Shi, X. Wang, W. Zhang, H. Yun, C. Lin, L. Chrostowski, and N. A. F. Jaeger, "Grating-coupled silicon microring resonators," *Appl. Phys. Lett.*, vol. 100, no. 12, Mar. 2012, Art. no. 121118.
[42] P. L. A. J. P. Hugonin, "High-order effective-medium theory of subwavelength gratings in classical mounting: Application to volume holograms," *J. Opt. Soc. Amer. A, Opt. Image Sci.*, vol. 15, pp. 1842–1851, Jul. 1998.
[43] J. Heebner, R. Grover, and T. Ibrahim, *Optical Microresonators: Theory, Fabrication and Applications*, 1st ed. London, U.K.: Springer, 2008.
[44] A. Yariv and P. Yeh, *Photonics: Optical Electronics in Modern Communications* (The Oxford Series in Electrical and Computer Engineering). London, U.K.: Oxford Univ. Press, 2006.
[45] P. Cheben, V. Donzella, S. Talebi Fard, L. Chrostowski, J. Schmid, C. Boudoux, L. R. Chen, A. Delâge, S. Janz, R. Kashyap, D. J. Lockwood, H.-P. Loock, and Z. Mi, "Study of waveguide crosstalk in silicon photonics integrated circuits," *Proc. SPIE*, vol. 8915, Oct. 2013, Art. no. 89150Z.
[46] S. Chandran, R. K. Gupta, and B. K. Das, "Dispersion enhanced critically coupled ring resonator for wide range refractive index sensing," *IEEE J. Sel. Topics Quantum Electron.*, vol. 23, no. 2, pp. 424–432, Mar. 2017.
[47] X. Chen and H. K. Tsang, "Polarization-independent grating couplers for silicon-on-insulator nanophotonic waveguides," *Opt. Lett.*, vol. 36, pp. 796–798, Dec. 2011.
[48] S. M. Rytov, "Electromagnetic properties of a finely stratified medium," *Sov. Phys.*, vol. 2, pp. 466–475, Dec. 1956.
[49] X. Xu, H. Subbaraman, J. Covey, D. Kwong, A. Hosseini, and R. T. Chen, "Complementary metal–oxide–semiconductor compatible high efficiency subwavelength grating couplers for silicon integrated photonics," *Appl. Phys. Lett.*, vol. 101, no. 3, Jul. 2012, Art. no. 031109.
[50] Y. Xiong, J. G. Wangàemert-Pérez, D.-X. Xu, J. H. Schmid, P. Cheben, and W. N. Ye, "Polarization splitter and rotator with subwavelength grating for enhanced fabrication tolerance," *Opt. Lett.*, vol. 39, no. 24, pp. 6931–6934, Dec. 2014.

[51] V. Donzella, A. Sherwali, J. Flueckiger, S. M. Grist, S. T. Fard, and L. Chrostowski, "Design and fabrication of SOI micro-ring resonators based on sub-wavelength grating waveguides," *Opt. Exp.*, vol. 23, pp. 4791–4803, Feb. 2015.
[52] C. Sciancalepore, B. B. Bakir, X. Letartre, J. Harduin, N. Olivier, C. Seassal, J.-M. Fedeli, and P. Viktorovitch, "CMOS-compatible ultra-compact 1.55-μm emitting VCSELs using double photonic crystal mirrors," *IEEE Photon. Technol. Lett.*, vol. 24, no. 6, pp. 455–457, Mar. 15, 2012.
[53] M. Martin and G. Cunge, "Surface roughness generated by plasma etching processes of silicon," *J. Vac. Sci. Technol. B, Microelectron. Nanometer Struct.*, vol. 26, no. 4, p. 1281, 2008.
[54] S. T. Fard, V. Donzella, S. A. Schmidt, J. Flueckiger, S. M. Grist, P. T. Fard, Y. Wu, R. J. Bojko, E. Kwok, N. A. F. Jaeger, D. M. Ratner, and L. Chrostowski, "Performance of ultra-thin SOI-based resonators for sensing applications," *Opt. Exp.*, vol. 22, no. 12, p. 14166, Jun. 2014.
[55] L. F. Hoyt, "New table of the refractive index of pure glycerol at 20°C," *Ind. Eng. Chem.*, vol. 26, no. 3, pp. 329–332, Mar. 1934.
[56] L. Huang, H. Tian, J. Zhou, Q. Liu, P. Zhang, and Y. Ji, "Label-free optical sensor by designing a high-Q photonic crystal ring–slot structure," *Opt. Commun.*, vol. 335, pp. 73–77, Jan. 2015.
[57] Y.-N. Zhang, Y. Zhao, and Q. Wang, "Measurement of methane concentration with cryptophane e infiltrated photonic crystal microcavity," *Sens. Actuators B, Chem.*, vol. 209, pp. 431–437, Mar. 2015.

LIJUN HUANG received the Ph.D. degree in information and communication engineering from the Beijing University of Posts and Telecommunications. He was a Visiting Scholar with the Microelectronics Research Center, The University of Texas at Austin, TX, USA, from 2015 to 2017. He currently works with the Key Laboratory of Intelligent Control Technology for Wuling-Mountain Ecological Agriculture in Hunan Province and the School of Electrical and Information Engineering, Huaihua University, China. His current research interest includes the design, fabrication, and characterization of silicon photonic devices for the optical interconnects and sensing in ecological agriculture.

HAI YAN received the Ph.D. degree in electrical and computer engineering from The University of Texas at Austin, TX, USA, in 2017. His research interests include the design, fabrication, and characterization of silicon photonic devices for biomedical sensing and optical interconnects.

LA XIANG was born in Hunan, China. She received the M.S. degree in electronics and communications engineering from the School of Electrical and Information Engineering, Hunan University, Hunan, in 2016. Her current research interest includes optical sensors and detection.

NI ZHOU was born in Hunan, China. She received the M.S. degree in electronics and communications engineering from the School of Electrical and Information Engineering, Hunan University, Hunan, in 2014. Her current research interest includes optical communication and sensors.

DAJIANG HE was born in Hunan, China. He received the Ph.D. degree from the School of Electrical and Information Engineering, Hunan University, Hunan, in 2009. He currently works with the Key Laboratory of Intelligent Control Technology for Wuling-Mountain Ecological Agriculture in Hunan Province, Huaihua University. His current research interest includes sensing and detection in ecological agriculture.

XIANWU MI was born in Hunan, China. He received the Ph.D. degree in microelectronics and solid state electronics from the Shanghai Institute of Microsystems and Information Technology, Chinese Academy of Sciences, Shanghai, China, in 2006. He currently works with the Key Laboratory of Intelligent Control Technology for Wuling-Mountain Ecological Agriculture in Hunan Province, Huaihua University. His current research interest includes optical sensing and devices in ecological agriculture.